Electronic origin of the conductivity imbalance between covalent and ionic amorphous semiconductors

Hui-Xiong Deng, Su-Huai Wei, Shu-Shen Li, Jingbo Li, and Aron Walsh

Phys. Rev. B **87**, 125203 — Published 21 March 2013

DOI: 10.1103/PhysRevB.87.125203

Electronic origin of the conductivity imbalance between covalent and ionic amorphous semiconductors

Hui-Xiong Deng and Su-Huai Wei

National Renewable Energy Laboratory, Golden, CO 80401, USA

Shu-Shen Li and Jingbo Li

State Key Laboratory for Superlattices and Microstructures,

Institute of Semiconductors, Chinese Academy of Sciences,

P. O. Box 912, Beijing 100083, China

Aron Walsh

Centre for Sustainable Chemical Technologies and Department of Chemistry,

University of Bath, Claverton Down, Bath BA2 7AY, United Kingdom

Abstract

Amorphous semiconductors are known to give rise to greatly reduced conductivity relative to their crystalline counterparts, which makes the recent development of amorphous oxide semiconductors with high electron mobility unexpected. Using first-principles molecular dynamics and electronic structure simulations, we have analyzed the electronic and optical properties of covalent and ionic oxide amorphous semiconductors. We observe that in covalent systems, amorphization introduces deep defect states inside the gap, resulting in a substantial deterioration of electrical conductivity. In contrast, in ionic systems, such as the transparent conducting oxide ZnO, amorphization does not create deep carrier-recombination centers, so the oxides still exhibit good conductivity and visible transparency relative to the crystalline phases. The origin of the conductivity imbalance between covalent and ionic amorphous semiconductors can be explained using a band coupling mechanism.

PACS numbers: 71.23.-k, 71.23.Cq, 78.20.Bh, 78.66.Jg, 71.15.Mb

A. INTRODUCTION

As an important component in thin-film transistors, flat-panel displays, electrochromic windows, and solar cells[1–5], transparent conducting oxides (TCOs), which uniquely combine high levels of conductivity with transmission of visible light, have attracted great attention in the past two decades. Recently, research in this field has focused more on amorphous TCOs (a-TCOs) because they offer potential advantages over conventional crystalline materials, such as low-cost synthesis, smooth surfaces, and accommodation to lattice strain. More importantly, unlike conventional covalent semiconductors, excellent optical transparency and conductivity can exist in a-TCOs even without chemical passivation[6]. It is generally expected that due to the lack of translational symmetry and the formation of dangling bond states, amorphous materials should exhibit a substantial deterioration in conductivity and optical transmittance. This is indeed observed in conventional covalent amorphous semiconductors (CAS), such as amorphous Si (a-Si) and Ge (a-Ge), in which electrical conductivity in the amorphous phase is several orders of magnitude lower than the crystalline phase[7,8]. Thus, it is quite surprising that a-TCOs and their alloys, such as a-ZnO, a-In_2O_3, a-$(In_2O_3)_x(ZnO)_{1-x}$ (a-IZO), a-$(In_2O_3)_x(SnO_2)_{1-x}$ (a-ITO), and a-$(SnO_2)_x(ZnO)_{1-x}$ (a-TZO), can still exhibit a high performance comparable to their crystalline counterparts[6,9–12].

To understand this puzzling observation and its underlying physics, we have performed first-principles calculations to study the electronic and optical properties of a-TCOs and compared them to traditional CAS. We find that the high conductivity in a-TCO materials is due to the high ionicity of the oxides: amorphization does not create deep levels inside the band gap, thus the conductivity and transparency are not significantly affected. This physical behavior is explained through a band coupling mechanism, which provides a fundamental understanding that will be useful for the future design of optoelectronic materials.

B. METHOD OF CALCULATIONS

Ab initio molecular dynamics (MD) simulations were performed using the Perdew-Burke-Ernzerhof (PBE) exchange-correlation functional[14] within density functional theory (DFT) as implemented in the code VASP[15–17]. The cutoff energy for the wavefunction expansion is 450 eV. Convergence with respect to the plane-wave cutoff energy and k-point sampling has

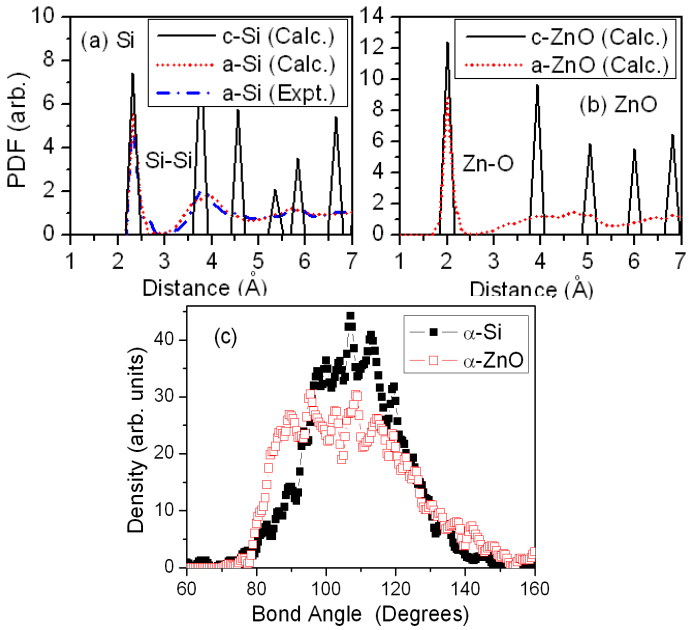

FIG. 1. (Color online) Calculated (Calc.) pair distribution functions (PDF) of (a) c-Si and a-Si, and (b) c-ZnO and a-ZnO, along with (c) bond-angle distributions of a-Si and a-ZnO. Experimental (Expt.) results from reference 13 are also plotted for comparison.

been carefully checked. The atomic-like core states are used to align the eigenvalue spectra of the crystalline and amorphous phases.

It is well-known that semi-local exchange-correlation functionals such as PBE underestimate the band gaps of semiconductors[18]. To provide more quantitative electronic and optical properties, we have also employed the non-local Heyd-Scuseria-Ernzerhof (HSE06) functional[19,20]. To illustrate the differences in the electronic structures of covalent and ionic oxides on amorphization, we choose the prototype covalent compound Si and ionic compound ZnO as examples. For crystalline Si (c-Si), the HSE06 calculated fundamental band gap with mixing coefficient $\alpha = 0.25$ is 1.16 eV, which is in good agreement with the experimental value of 1.12 eV. For crystalline ZnO (c-ZnO), the HSE06 calculated band gap with mixing coefficient $\alpha = 0.375$ is 3.40 eV for the wurtzite (WZ) structure (3.24 eV for zinc-blende (ZB) structure), also in good agreement with the experimental value of 3.44 eV[21].

To generate the amorphous structures, MD simulations were carried out on a cubic supercell of 216 atoms for both Si and ZnO. The k-point sampling was restricted to the Γ point. Amorphization is realized following a four-step process[22,23]: (i) Heating the crys-

talline structure to generate the melted phase at a temperature of 2500 K within Nosé canonical ensemble, using a time step of 3 fs. (ii) After equilibration at 2500K, the temperature was quenched to 2000 K for 4 ps using a time step of 2 fs. (iii) After equilibration at 2000K, the temperature was quenched to 1500 K at the same cooling rate. (iv) The same process was repeated towards 0 K, where a standard geometry relaxation was performed and the lattice constant was optimised to zero pressure.

C. RESULTS AND DISCUSSIONS

Figure 1 shows the calculated pair distribution functions (PDF) and bond-angle distributions of a-Si and a-ZnO structures produced by MD simulations. We notice that the first coordination shell of a-Si and a-ZnO matches the first peak of their respective crystalline phase. Outside the first coordination shell, as expected, no long-range order is observed for the amorphous phase. It is also clear from Fig. 1(a) that the simulated PDF of a-Si well agrees with the experimental measurement. To avoid the issue of the coordination number depending on the choice of radius, we adopt the concept of effective coordination number (ECN)[23,24] to obtain the average coordination number, i.e.

$$ECN_i = \sum_j \exp[1 - (\frac{r_{i,j}}{r^i_{av}})^6] \tag{1}$$

Here r^i_{av} is defined as:

$$r^i_{av} = \frac{\sum_j r_{i,j} \exp[1 - (\frac{r_{i,j}}{r^i_{min}})^6]}{\sum_j \exp[1 - (\frac{r_{i,j}}{r^i_{min}})^6]} \tag{2}$$

$r_{i,j}$ and r^i_{min} are the bond length and minimum bond length between the atom i and the surrounding atoms. Thus, the average coordination number can be obtained by

$$\bar{N} = \frac{1}{M} \sum_i^M ECN_i \tag{3}$$

Where M is the number of atoms. Table I shows the simulated structural parameters of a-Si and a-ZnO, where they are compared to the corresponding experimental data when possible. For a-Si, the obtained average coordination ($\bar{N}$) number of 3.985 is similar to that obtained by integration to the first minimum in the PDF. It is seen that the simulated average coordination number and first-neighbor distance ($\bar{r}$) are very close to the corresponding values in crystalline phases. On the other hand, the bond angles (θ) are mostly distributed between

80° to 140° (Fig. 1(c)), with a mean value ($\bar{\theta}$) of 108.6° and standard deviation (σ_θ) of 14.3°, consistent with previous simulations[25,26]. Compared with experimental studies, these simulated structural parameters are in good agreement with x-ray and neutron measurements for a-Si[27,28]. For a-ZnO, the average coordination number is 3.82, well in agreement with previous prediction[23]. The mean bond angle is 108.9° with a standard deviation of 18.4°, slightly smaller than the tetrahedral angle of 109.47° in crystalline phase. It is clearly seen that the average coordination number is slightly smaller and the standard deviation of bond angles of a-ZnO is larger than those of a-Si. This indicates that the generated a-ZnO structure is more disordered than a-Si. The structure generation process was carried out several times using different quenching rates, and we found that the qualitative results are insensitive to the choice of the amorphous phases[23,29].

TABLE I. Structural parameters of a-Si and a-ZnO: average coordination number ($\bar{N}$), mean first-neighbor distance ($\bar{r}$), standard deviation of bond lengths(σ_r), mean bond angle ($\bar{\theta}$) and standard deviation of bond angles(σ_θ).

		$\bar{N}/4$		$\bar{r}$(Å)	σ_r(Å)	$\bar{\theta}$ (deg)	σ_θ (deg)
a-Si	Theory	0.996[a]		2.38[a]	0.04[a]	108.6[a]	14.3[a]
		1.007[b]		2.38[b]	0.08[b]	108.3[b]	15.5[b]
		0.963[c]		–	–	109.1[c]	12.5[c]
	Experiment	0.99(3)[d]	0.975[e]	2.36[d]	0.07[d]	108.6[e]	11.0[e]
a-ZnO	Theory	0.955[a]		2.01[a]	0.05[a]	108.9[a]	18.4[a]

[a]This work; [b]Reference[25]; [c]Reference[26]; [d]Reference[27]; [e]Reference[28].

Figures 2(a) and (b) show the band structures and total density of states (DOS) of the c-Si and a-Si supercells, respectively. It is clearly seen that the amorphization of Si introduces many deep defect states inside the band gap, leading to a large reduction of the effective band gap. Figures 3(a)-(d) present the charge density isosurfaces of the band edge states of c-Si and a-Si. As expected, both the conduction band minimum (CBM) and valence band maximum (VBM) states of c-Si are extended over the whole crystal. This is why c-Si could have excellent n-type or p-type conductivity after doping. However,

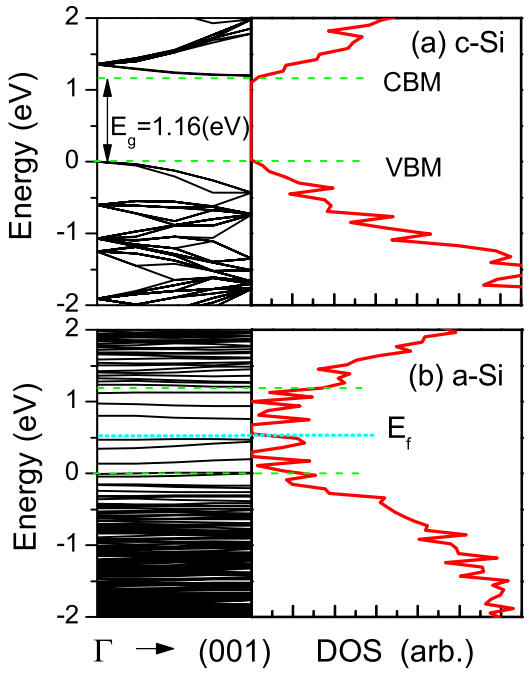

FIG. 2. (Color online) Band structures (left) and total density of states (right) of (a) c-Si and (b) a-Si systems based on HSE06 calculations. Green dashed lines show the band edges of c-Si. The energy of the valence band maximum of c-Si is set to be 0 eV for each case. Cyan dotted lines indicate the Fermi level (E_f) position in the a-Si system.

in the a-Si phase, the lowest unoccupied band (LUB) and highest occupied band (HOB) derived from the dangling bond states are strongly localized [Figs. 3(b) and (d)], which would act as both electron and hole traps, causing recombination of carriers, and reducing the conductivity. Consequentially, the amorphization of Si is associated with a substantial deterioration in electrical conductivity, as observed experimentally[8]. We have also verified that this situation is true for some other covalent amorphous compounds. For example, figure 4 presents the band structures of amorphous Ge and GaAs (a-GaAs). It is similarly found that the amorphization of Ge and GaAs also introduces many deep defect states inside the band gap, consequently leading to a substantial deterioration of electrical conductivity.

The band structures of c-ZnO and a-ZnO are plotted in Figs. 5 (a) and (b), respectively. Compared to the crystalline phase, amorphization only slightly raises the valence band (i.e., 0.32 eV higher in energy than that of c-ZnO), and the conduction band onset is almost unchanged. So, stoichiometric a-ZnO still has a large fundamental band gap of 2.84 eV. As the dominant intrinsic defects in a-ZnO are the dangling bonds of Zn and O atoms, these

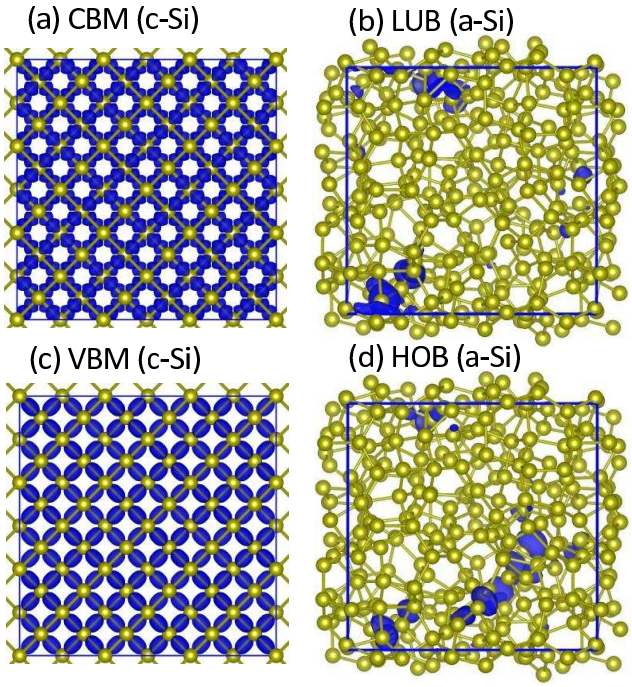

FIG. 3. (Color online) Band decomposed charge density isosurfaces of band edge states of c-Si (a and c) and a-Si (b and d). The yellow balls depict the Si atoms.

results demonstrate that cation and anion dangling bond states are shallow. Therefore a-ZnO is unlikely to form deep recombination centers through dangling bond states, and hence a high conductivity could be achieved, in contrast to the a-Si system (Fig. 2). The calculated optical absorption coefficients α of c-ZnO and a-ZnO are shown in Figs. 5(c) and (d), respectively. We find that for the crystalline phase, the optical band gap is almost equal to the fundamental band gap, whereas for the amorphous phase, the optical band gap is about 3.12 eV, i.e., 0.28 eV larger than the fundamental band gap because of the weak absorption associated with the band tail states[23,30]. The preservation of the large band gap is in good agreement with recent measurements[31]. Although amorphization creates many defects and dangling bonds in ZnO, due to the high electronegativity of the oxygen relative to Zn, a-ZnO still has a large fundamental band gap and excellent optical transmittance to visible light. We have confirmed that a-ZnO generated from the WZ structure, instead of a ZB lattice, exhibits similar electronic and optical behavior.

The charge density of the band edge states from a-ZnO is shown in Fig. 6. The LUB state is highly delocalized, which is significantly different from a-Si [Figs. 3(b)]. In contrast, the HOB is localized. The reason can be understood as follows. For TCOs such as ZnO the

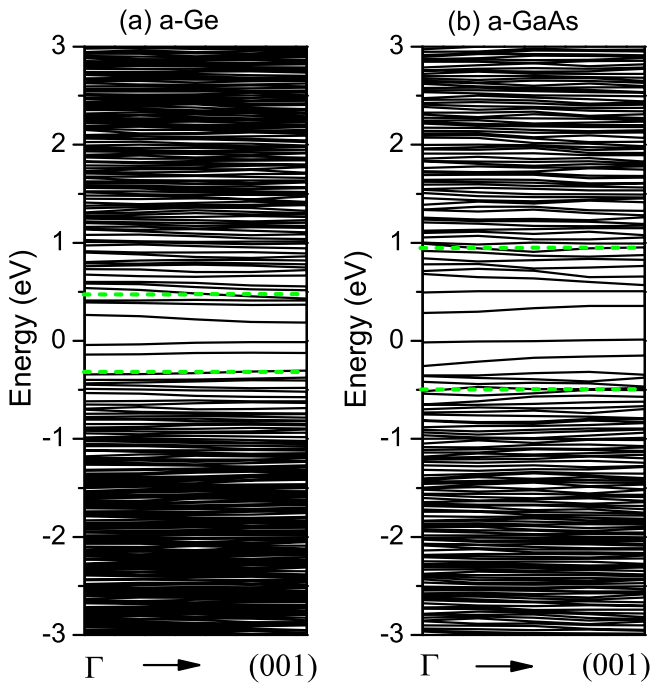

FIG. 4. (Color online) Band structures of (a) a-Ge and (b) a-GaAs based on HSE06 calculations. The highest occupied states are set to 0 eV. The dashed green lines show the band edges of corresponding crystalline phase for each case.

lowest conduction bands primarily consist of cation s and anion s orbitals. These orbitals have a large isotropic radial distribution, which is not sensitive to the structural variations of the amorphous phase[3]. However, due to a combination of the high electronegativity of oxygen and the anisotropic orbital overlap, the O $2p$ derived valence band top states of a-ZnO are always very localized (Fig. 6(b)). Despite the presence of VBM-derived dangling bond states in a-TCOs, these states do not act as deep levels to trap electron carriers, and hence in amorphous TCOs, such as a-ZnO, a-In_2O_3, and a-SnO_2, high levels of electron conductivity can still be maintained. It is therefore possible to understand why a-TCOs maintain a high performance relative to the crystalline phase, as observed in many experimental studies.

In order to provide a clearer physical understanding of the electronic origin of the conductivity imbalance between covalent and ionic amorphous systems, we illustrate the process of the formation of the dangling bond states in a-Si [Fig. 7(a)] and a-ZnO [Fig. 7(b)]. In the CAS systems, such as Si, Ge, and even GaAs, each elemental component has the same or similar atomic orbital energies. When they form a bond in the solid-state, there is strong coupling between the energy levels of neighboring atoms. Consequently, the band

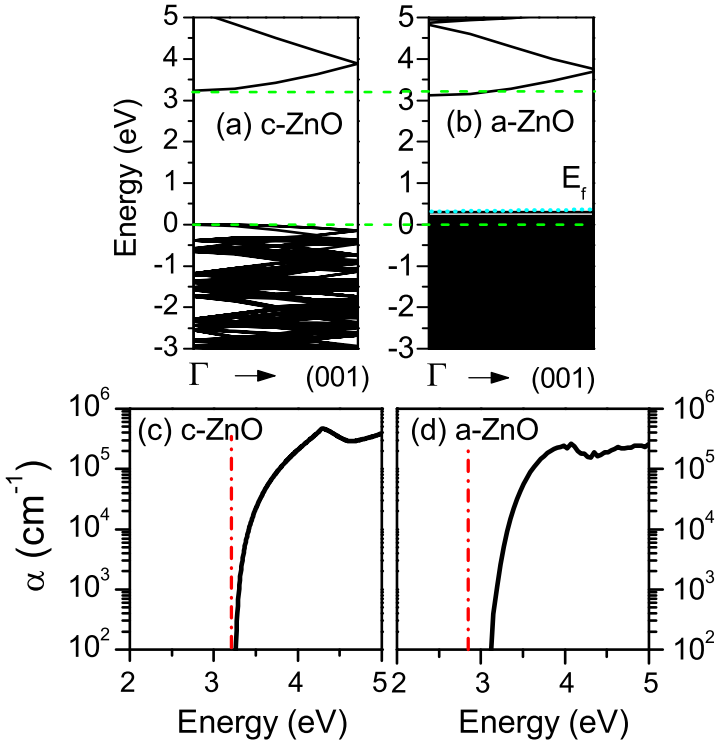

FIG. 5. (Color online) Band structures of (a) c-ZnO and (b) a-ZnO based on HSE06 calculations. The highest occupied state of c-ZnO is set to 0 eV. The Fermi level (E_f) in a-ZnO is indicated by the horizontal cyan dotted line. Optical absorption coefficients α of (c) c-ZnO and (d) a-ZnO are also shown. The vertical red dot-dashed line indicates the location of the fundamental band gap for each case.

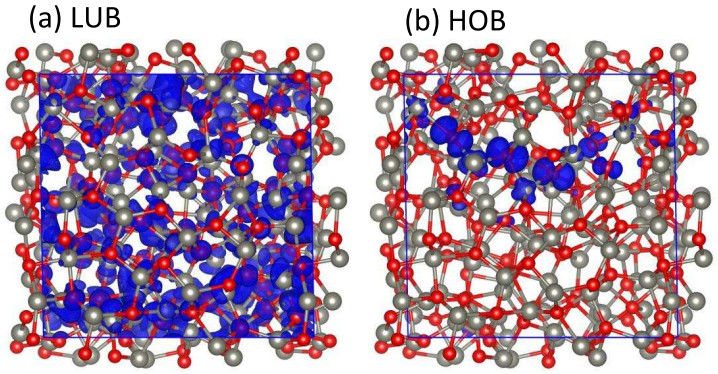

FIG. 6. (Color online) Band decomposed charge density isosurfaces of (a) LUB and (b) HOB of a-ZnO. Zn and O atoms are colored gray and red, respectively.

gap is formed mainly between the antibonding and bonding states of the host atomic energy

levels. However, when a dangling bond is created in the amorphous phase, the resulting energy level is almost restored to the atomic value, and is hence located at the center of the band gap. This process induces a deep defect level, as shown in Fig. 7(a) for the case of a-Si. In contrast, for ionic oxides, the energy level difference between cations and anions is very large, so the band coupling and energy level repulsion are weak. Hence, when anion dangling bonds are created in the amorphous phase, the defect levels are close to the valence band of the host, while for cation dangling bonds, their defect levels are located close to the conduction band of the crystalline compound. Therefore, both disorder-induced defect levels are shallow for ionic systems. Because of the large electronegativity of oxygen, the electrons located on cation dangling bonds transfer to the unsaturated anion bonds, and accordingly a large band gap is still preserved for such ionic systems [Fig. 7(b)].

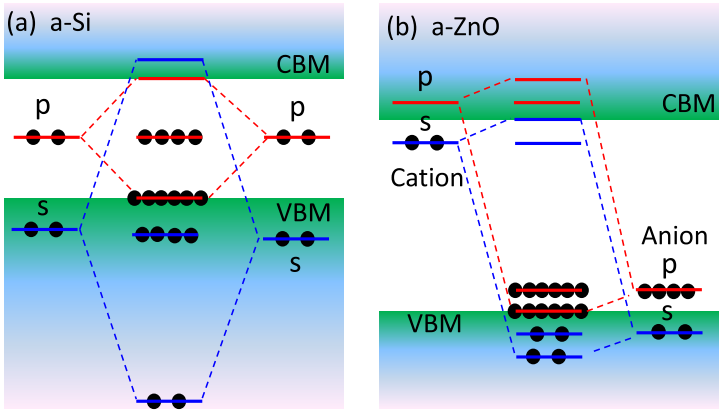

FIG. 7. (Color online) Schematic plot of the formation of the dangling bond states in (a) a-Si and (b) a-ZnO systems. The CBM and VBM represent the band edge energies of the host. The solid balls indicate the occupation of electrons.

D. CONCLUSIONS

In conclusion, we have analyzed the effects of amorphization on the electronic structure of covalent and ionic semiconductors. For covalent materials, amorphization induces dangling bond states that create localized deep defect levels, which act as both electron and hole traps. These states lead to a substantial reduction in conductivity compared to the crystalline material. In contrast, for ionic amorphous oxides the defect states induced by amorphization are shallow, so the changes in conductivity and optical transparency are not

to the detriment of carrier transport. The essential physics of these processes are captured in a band coupling mechanism based on the energies of the atomic orbitals involved. This understanding provides a promising way to engineer the conductivity and optical properties of amorphous materials for optoelectronic device applications.

E. ACKNOWLEDGMENTS

The work at NREL was supported by the U.S. Department of Energy under Contract No. DE-AC36-08GO28308. The work at IS, CAS was supported by the National Basic Research Program of China (973 Program) Grant No. G2009CB929300, and the National Natural Science Foundation of China under Grants No. 61121491, and No. 11104264.

---

[1] G. Thomas, Nature **389**, 907 (1997).

[2] J. F. Wager, Science **300**, 1245 (2003).

[3] K. Nomura, H. Ohta, A. Takagi, T. Kamiya, M. Hirano, and H. Hosono, Nature **432**, 488 (2004).

[4] E. Fortunato, D. Ginley, H. Hosono, and D. C. Paine, MRS Bull **32**, 242 (2007).

[5] A. Walsh, J. L. F. Da Silva, S. Wei, C. Körber, A. Klein, L. F. J. Piper, A. DeMasi, K. E. Smith, G. Panaccione, P. Torelli, D. J. Payne, A. Bourlange, and R. G. Egdell, Phys. Rev. Lett. **100**, 167402 (2008).

[6] M. P. Taylor, D. W. Readey, M. F. A. M. van Hest, C. W. Teplin, J. L. Alleman, M. S. Dabney, L. M. Gedvilas, B. M. Keyes, B. To, J. D. Perkins, and D. S. Ginley, Adv. Funct. Mater. **18**, 3169 (2008).

[7] D. Emin, Science **198**, 881 (1977).

[8] N. F. Mott, *Conduction in non-crystalline materials* (Oxford Science Publications, Oxford, 1987).

[9] H. Nakazawa, Y. Ito, E. Matsumoto, K. Adachi, N. Aoki, and Y. Ochiai, J. Appl. Phys. **100** (2006).

[10] E. Fortunato, A. Pimentel, A. Goncalves, A. Marques, and R. Martins, Thin Solid Films **502**, 104 (2006).

[11] Y. Shigesato and D. C. Paine, Appl. Phys. Lett. **62**, 1268 (1993).

[12] V. L. Kuznetsov, D. H. O'Neil, M. Pepper, and P. P. Edwards, Appl. Phys. Lett. **97**, 262117 (2010).

[13] S. Kugler, L. Pusztai, L. Rosta, P. Chieux, and R. Bellissent, Phys. Rev. B **48**, 7685 (1993).

[14] J. P. Perdew, K. Burke, and M. Ernzerhof, Phys. Rev. Lett. **77**, 3865 (1996).

[15] G. Kresse and J. Hafner, Phys. Rev. B **47**, 558 (1993).

[16] G. Kresse and J. Hafner, Phys. Rev. B **48**, 13115 (1993).

[17] G. Kresse and J. Furthmuller, Comput. Mater. Sci. **6**, 15 (1996).

[18] J. P. Perdew and M. Levy, Phys. Rev. Lett. **51**, 1884 (1983).

[19] J. Heyd, G. E. Scuseria, and M. Ernzerhof, J. Chem. Phys. **118**, 8207 (2003).

[20] J. Paier, M. Marsman, K. Hummer, G. Kresse, I. C. Gerber, and J. G. Ángyán, J. Chem. Phys. **124**, 154709 (2006).

[21] O. Madelung, *Semiconductors: Data Handbook* (Springer, Berlin, 2004).

[22] M. D. Kluge, J. R. Ray, and A. Rahman, Phys. Rev. B **36**, 4234 (1987).

[23] A. Walsh, J. L. F. Da Silva, and S. Wei, Chem. Mater. **21**, 5119 (2009).

[24] R. Hoppe, Angew. Chem. Int. Ed. Engl. **9**, 25 (1970); R. Hoppe, S. Voigt, H. Glaum, J. Kissel, H. P. Muller, and K. Bernet, J. Less-Common Met. **156**, 105 (1989).

[25] I. Štich, R. Car, and M. Parrinello, Phys. Rev. B **44**, 11092 (1991).

[26] P. Biswas, R. Atta-Fynn, and D. A. Drabold, Phys. Rev. B **69**, 195207 (2004); D. A. Drabold, P. A. Fedders, O. F. Sankey, and J. D. Dow, Phys. Rev. B. **42**, 5135 (1990); J. Dong and D. A. Drabold, Phys. Rev. Lett. **80**, 1928 (1998).

[27] M. Benfatto, C. R. Natoli, and A. Filipponi, Phys. Rev. B **40**, 9626 (1989); A. Filipponi, F. Evangelisti, M. Benfatto, S. Mobilio, and C. R. Natoli, Phys. Rev. B. **40**, 9636 (1989).

[28] J. Fortner and J. S. Lannin, Phys. Rev. B **39**, 5527 (1989).

[29] A. Walsh, J. L. F. Da Silva, and S. Wei, J. Phys.: Condens. Matter **23**, 334210 (2011).

[30] D. L. Wood and J. Tauc, Phys. Rev. B **5**, 3144 (1972).

[31] J. Khoshman and M. Kordesch, Thin Solid Films **515**, 7393 (2007).